PERGAMON

International Journal of Solids and Structures 38 (2001) 5865–5892

INTERNATIONAL JOURNAL OF SOLIDS and STRUCTURES

www.elsevier.com/locate/ijsolstr

Isotropic damage model with different tensile–compressive response for brittle materials

A. Brencich, L. Gambarotta *

Department of Structural and Geotechnical Engineering, University of Genova, via Montallegro 1, 16145 Genova, Italy

Received 22 May 2000; in revised form 11 October 2000

Dedicated to Prof. Giovanni Alpa for his 60th birthday

Abstract

Incremental constitutive equations for brittle materials are formulated on the grounds of a frictional microcracked elastic model. The hypothesis of isotropic damage and the description of normal and tangential contact tractions on the crack faces by means of two second-order tensors provide a constitutive model with a reduced number of internal variables. The evolution equations of the latter ones are deduced from frictional and damage limit states and corresponding flow rules, from which the different behaviour to tensile and compressive stress states and dissipation at constant damage are represented. The model response is analysed for different stress states and limit strength domains are derived for monotonically increasing biaxial and triaxial stress states. Comparisons of the theoretical results with experimental data from literature related to concrete and cast-iron corroborate the proposed approach.

Keywords: Brittle materials; Damage model; Constitutive equations; Limit strength domains

1. Introduction

Constitutive modelling of brittle materials implies different problems, among which the description of the different response to tensile, compressive and mixed stress states, which have been tackled by means of either phenomenological approaches, mainly based on experimental grounds, or micromechanical descriptions of the material structure.

Phenomenological models, involving a limited number of internal variables, have been derived from the plasticity theory (Chen, 1982; Hsieh et al., 1982; Pietruszczak et al., 1988; Etse and Willam, 1995; Lee and Willam, 1997; Winnicki and Cichon, 1998) and from the damage theory (Lemaitre, 1992; Krajcinovic, 1996). In the frame of Continuum Damage Mechanics, material degradation is represented at different levels of detail by scalar, vectorial and tensorial variables for isotropic and anisotropic formulations,

* Corresponding author. Address: Facoltà di Ingegneria, DISEG, via Montallegro 1, 16145 Genova, Italy. Tel.: +39-010-353-2517; fax: +39-010-353-2534.

E-mail address: gambarotta@diseg.unige.it (L. Gambarotta).

0020-7683/01/$ - see front matter
PII: S0020-7683(00)00386-3

respectively. Moreover, the different tensile–compressive response and the dissipation phenomena at constant damage have been described by means of the concept of positive and negative projections of stress and strain tensors (Ortiz, 1985; Chaboche, 1992, 1993; Lubarda et al., 1994; Hansen and Schreyer, 1995) and by coupled damage plasticity models (Lubliner et al., 1989; Yazdani and Schreyer, 1988, 1990; Abu-Lebdeh and Voyiadjis, 1993).

A deeper insight and representation of these phenomena may be given by the micromechanical models based on a description of the meso-structure as a population of microcracks embedded in an elastic matrix (Kachanov, 1982; Bazant and Prat, 1988; Fanella and Krajcinovic, 1988; Nemat-Nasser and Obata, 1988 Gambarotta and Lagomarsino, 1993; Prat and Bazant, 1997; Basista and Gross, 1998 Lawn and Marshall, 1998). A possible formulation assumes non-interacting plane microcracks gathered into sets of selected orientations, implying the damage representation to be based on a proper distribution of axial vectors. In this way the unilateral frictional mechanisms induced by compressive stress states on crack faces may be easily taken into account, so providing a direct interpretation to the different response to tensile and compressive stress states, load induced anisotropy and energy dissipation at constant damage (Gambarotta and Lagomarsino, 1993). On the other hand, the main drawback of these models consists of the high number of internal variables involved and the related computational difficulties. As a consequence, some attempts have been made to formulate constitutive models characterised by a limited number of internal variables and based on a micromechanical ground (Krajcinovic et al., 1991; Halm and Dragon, 1998).

In the present paper a damage model for brittle materials with a limited number of internal variables is proposed, developed on the basis of the model by Gambarotta and Lagomarsino (1993). Damage is assumed to be isotropic, i.e. independent of the crack orientation, and the unilateral frictional conditions on the crack faces are considered on the average. This allows damage to be represented by a scalar variable and the crack opening/sliding effects by two second-order tensors related to the overall normal and tangential tractions on the crack faces. The evolution of the internal variables are ruled by two limit conditions concerning damage propagation and an average sliding rule of Drucker–Prager type (Drucker and Prager, 1952). Constitutive equations are derived in incremental form and limit strength domains are obtained. The model response is discussed with reference to relevant stress states and the limit strength domains for two and three-axial stress states are discussed and compared with experimental data from literature. Even though the validity of the proposed model is limited by the assumption of isotropic damage, nevertheless the present approach could be useful for deriving constitutive equations for materials undergoing anisotropic damage as well. An example can be found in Brencich and Gambarotta (1998) where anisotropic damage of frictionless microcracked elastic solids is considered.

2. Isotropic damage model

Brittle and quasi-brittle materials are commonly modelled as microcracked solids in which damage may be described through the propagation of plane cracks embedded in an elastic matrix. Following the approach by Gambarotta and Lagomarsino (1993), the constitutive equation may be expressed by defining the mean strain $\mathbf{E}$ tensor as the sum of the mean strain in the elastic matrix and the contributions due to the displacement discontinuities across the crack faces:

$$\mathbf{E} = \mathbf{K}\mathbf{T} + \frac{1}{2\pi}\int_{\Omega} [\varepsilon \mathbf{n} \otimes \mathbf{n} + \mathrm{sym}(\boldsymbol{\gamma} \otimes \mathbf{n})]\, \mathrm{d}\Omega, \tag{1}$$

where $\mathbf{K}$ is the fourth-order elastic compliance tensor of the matrix and $\mathbf{T}$ is the mean stress tensor; ε and $\boldsymbol{\gamma}$ are, respectively, the normal extension and the tangential sliding vector related to the subset of microcracks with normal contained inside the neighbourhood of the unit vector $\mathbf{n}$ with amplitude measured by the infinitesimal solid angle $\mathrm{d}\Omega$ on the unit hemisphere Ω of all orientations.

Under the hypothesis of non-interacting and self-similar propagating cracks, ε and $\boldsymbol{\gamma}$ can be expressed as functions of the resolved stresses $\sigma = \mathbf{n} \cdot \mathbf{T}\mathbf{n}$ and $\boldsymbol{\tau} = (\mathbf{I} - \mathbf{n} \otimes \mathbf{n})\mathbf{T}\mathbf{n}$ on the $\mathbf{n}$-plane and of the normal and tangential components p and $\mathbf{f}$ of the contact tractions on the crack faces as follows:

$$\varepsilon = c_n \alpha^3 (\sigma - p), \tag{2a}$$

$$\boldsymbol{\gamma} = c_t \alpha^3 (\boldsymbol{\tau} - \mathbf{f}), \tag{2b}$$

where c_n and c_t can be regarded as compliance parameters related to microcracks and the ratio $\alpha = a/a_o$ between the actual crack average size a and the original one a_o as the damage variable of the $\mathbf{n}$-oriented plane. According to this approach, α, p and $\mathbf{f}$ play the role of internal variables related to the orientation $\mathbf{n}$. If dilatancy is neglected during the sliding on compressed planes, the unilateral contact between the crack faces may be expressed in terms of a linear complementarity problem (LCP) for ε and p:

$$\varepsilon \geqslant 0, \quad p \geqslant 0, \quad p\varepsilon = 0 \tag{3}$$

from which, together with definition (2a), it turns out that the normal contact traction p only depends on the stress tensor $\mathbf{T}$ in terms of the McAuley operator as follows:

$$p = -\langle -\sigma \rangle. \tag{4}$$

Once the dependence of the internal variables α and $\mathbf{f}$ on the load history is known, the mean strain tensor $\mathbf{E}$ can be evaluated by substituting Eqs. (2a) and (2b) into Eq. (1):

$$\mathbf{E} = \mathbf{K}\mathbf{T} + \frac{1}{2\pi} \int_\Omega c_n \alpha^3 (\sigma - p)\mathbf{n} \otimes \mathbf{n}\, \mathrm{d}\Omega + \frac{1}{2\pi} \int_\Omega c_t \alpha^3 \,\mathrm{sym}[(\boldsymbol{\tau} - \mathbf{f}) \otimes \mathbf{n}]\, \mathrm{d}\Omega. \tag{5}$$

Eq. (5) points out that the contributions to the mean strain associated to the direction $\mathbf{n}$ are due both to the effective normal $(\sigma - p)$ and shear $(\boldsymbol{\tau} - \mathbf{f})$ tractions acting on the $\mathbf{n}$-oriented plane, here also called damage plane.

Computation of the mean strain components from Eq. (5) needs the integration over the unit hemisphere of all orientations Ω, that can be approximated by the sum of the contributions related to a discrete number of orientations $\mathbf{n}$. The main limit of this description is given by the large number of internal variables that have to be managed and recorded, so implying an extraordinary computational effort.

In the following, reference is made to materials that are isotropic at their natural state, e.g. the inelastic compliance coefficients c_n and c_t and the initial crack length a_o take the same value at every orientation $\mathbf{n}$. Moreover, damage is assumed to be isotropic in the whole deformation process assuming the same value for the damage variable α on every damage plane.

As a consequence, the additional strain due to microcracks is represented by two contributions, the first one due to the extensions

$$\mathbf{E}_{\mathrm{n}}^* = c_n \alpha^3 \int_\Omega (\sigma - p)\mathbf{n} \otimes \mathbf{n}\, \mathrm{d}\Omega = c_n \alpha^3 (\mathbf{H}_{\mathrm{n}}\mathbf{T} - \mathbf{P}) \tag{6a}$$

and the second one related to the slidings:

$$\mathbf{E}_{\mathrm{t}}^* = c_t \alpha^3 \int_\Omega \mathrm{sym}[(\boldsymbol{\tau} - \mathbf{f}) \otimes \mathbf{n}]\, \mathrm{d}\Omega = \tilde{c}_{\mathrm{t}} \alpha^3 \left(\mathbf{H}_{\mathrm{t}}\mathbf{T} - \mathbf{F}' \right) \tag{6b}$$

on the crack planes. These definitions imply the compliance coefficients to be replaced by:

$$c_{\mathrm{n}} = \frac{2\pi c_n}{3}, \qquad \tilde{c}_{\mathrm{t}} = \frac{2\pi c_t}{3}, \tag{7a, b}$$

and the second-order tensors $\mathbf{F}'$ and $\mathbf{P}$, and the fourth-order tensors $\mathbf{H}_{\mathrm{n}}$ and $\mathbf{H}_{\mathrm{t}}$ defined as follows:

$$\mathbf{P} = \frac{3}{2\pi}\int_{\Omega^-} p\mathbf{n}\otimes\mathbf{n}\,\mathrm{d}\Omega, \tag{7c}$$

$$\mathbf{F}' = \frac{3}{2\pi}\int_{\Omega} \mathrm{sym}(\mathbf{f}\otimes\mathbf{n})\,\mathrm{d}\Omega, \tag{7d}$$

$$\mathbf{H}_\mathrm{n}\mathbf{T} = \frac{3}{2\pi}\int_{\Omega} \sigma\mathbf{n}\otimes\mathbf{n}\,\mathrm{d}\Omega, \qquad \mathbf{H}_\mathrm{t}\mathbf{T} = \frac{3}{2\pi}\int_{\Omega} \mathrm{sym}(\boldsymbol{\tau}\otimes\mathbf{n})\,\mathrm{d}\Omega, \tag{7e, f}$$

where Ω^- is the set of compressed planes $\Omega^- = \{\mathbf{n}|\ |\mathbf{n}| = 1, \mathbf{n}\cdot\mathbf{T}\mathbf{n} < 0\}$.

The symmetric second-order tensors $\mathbf{P}$ and $\mathbf{F}'$ may be interpreted as the average effects on all the orientations of the normal and tangential contact tractions; moreover it can be proved that $\mathbf{F}'$ is traceless and $\mathrm{tr}\,\mathbf{P} \leqslant 0$. Correspondingly to the hypothesis of isotropic damage and in order to avoid the description of the frictional tractions $\mathbf{f}$ during the loading process, the definition of Eq. (7d) cannot be considered effective. This assumption implies the alternative choice of the tensor $\mathbf{F}'$ as an internal variable representative of the average frictional tractions.

The fourth-order tensors $\mathbf{H}_\mathrm{n}$ and $\mathbf{H}_\mathrm{t}$ are symmetric and isotropic, with components given as:

$$(\mathbf{H}_\mathrm{n})_{ijlm} = \frac{3}{2\pi}\int_{\Omega} n_i n_j n_l n_m\,\mathrm{d}\Omega, \tag{8a}$$

$$(\mathbf{H}_\mathrm{t})_{ijlm} = \frac{3}{8\pi}\int_{\Omega} \left(\delta_{im}n_l n_j + \delta_{il}n_m n_j + \delta_{jm}n_l n_i + \delta_{jl}n_m n_i\right)\mathrm{d}\Omega - (\mathbf{H}_\mathrm{n})_{ijlm}, \tag{8b}$$

moreover, by definition (7d), it results $\mathrm{tr}\,(\mathbf{H}_\mathrm{t}\mathbf{T}) = 0$. By integration of Eq. (7e,f) one obtains:

$$\mathbf{H}_\mathrm{n}\mathbf{T} = \frac{2}{5}\left(\mathbf{T} + \frac{3}{2}\mathrm{p}\mathbf{I}\right) = \frac{2}{5}\mathbf{T}' + \mathrm{p}\mathbf{I}, \tag{9a}$$

$$\mathbf{H}_\mathrm{t}\mathbf{T} = \frac{3}{5}(\mathbf{T} - \mathrm{p}\mathbf{I}) = \frac{3}{5}\mathbf{T}', \tag{9b}$$

being $\mathrm{p} = (\mathrm{tr}\,\mathbf{T})/3$ the hydrostatic pressure and $\mathbf{T}'$ the deviatoric stress tensor, respectively.

When triaxial compressive stress states are applied, the strain contribution $\mathbf{E}^*_\mathrm{n}$ due to crack opening vanishes and from Eq. (6a) it results $\mathbf{P} = \mathbf{H}_\mathrm{n}\mathbf{T}$. On the other hand, under triaxial tensile stresses the normal contact traction vanishes at every orientation and from Eq. (7c) it follows that $\mathbf{P} = \mathbf{0}$. Finally, for arbitrary stress states, the tensor $\mathbf{P}$ is obtained simply carrying out integration (7c). Once the global friction tensor $\mathbf{F}'$ is given, the inelastic strain due to sliding becomes independent of the hydrostatic component of the stress tensor $\mathbf{T}$; in fact in Eq. (9b) this component does not affect the linear transformation represented by tensor $\mathbf{H}_\mathrm{t}$. For this reason Eq. (6b) can be equivalently rewritten as:

$$\mathbf{E}^*_\mathrm{t} = \tilde{c}_\mathrm{t}\alpha^3\left(\mathbf{H}_\mathrm{t}\mathbf{T}' - \mathbf{F}'\right).$$

By defining the new tensors $\mathbf{P}^*$ and $\mathbf{F}^{*\prime}$ as follows:

$$\mathbf{P}^* = \mathbf{H}_\mathrm{n}^{-1}\mathbf{P} = \tfrac{5}{2}\mathbf{P} - \tfrac{1}{2}(\mathrm{tr}\,\mathbf{P})\mathbf{I}, \tag{10a}$$

$$\mathbf{F}^{*\prime} = \mathbf{H}_\mathrm{t}^{-1}\mathbf{F}' = \tfrac{5}{3}\mathbf{F}', \tag{10b}$$

the additional strains can be written in a form similar to Eqs. (2a) and (2b):

$$\mathbf{E}^*_\mathrm{n} = c_\mathrm{n}\alpha^3\mathbf{H}_\mathrm{n}(\mathbf{T} - \mathbf{P}^*), \tag{11a}$$

$$\mathbf{E}_{\mathrm{t}}^{*} = c_{\mathrm{t}}\alpha^{3}(\mathbf{T}' - \mathbf{F}^{*\prime}), \tag{11b}$$

where $c_{\mathrm{t}} = 3/5\tilde{c}_{\mathrm{t}}$. Tensors $\mathbf{P}^{*}$ and $\mathbf{F}^{*\prime}$ are given the same physical meaning as tensors $\mathbf{P}$ and $\mathbf{F}'$: for generic stress states $\mathrm{tr}\,\mathbf{P}^{*} = \mathrm{tr}\,\mathbf{P}$ and $\mathrm{tr}\,\mathbf{F}^{*\prime} = \mathrm{tr}\,\mathbf{F}' = 0$; in the case of triaxial compressive stress states tensors $\mathbf{P}^{*}$ and $\mathbf{T}$ coincide, while in the case of triaxial tensile stress states it follows $\mathbf{P}^{*} = \mathbf{0}$. The definitions provided by Eqs. (11a) and (11b) allow the constitutive equation to be expressed in terms of scalar and tensor entities:

$$\mathbf{E} = \mathbf{K}\mathbf{T} + c_{\mathrm{n}}\alpha^{3}\mathbf{H}_{\mathrm{n}}(\mathbf{T} - \mathbf{P}^{*}) + c_{\mathrm{t}}\alpha^{3}(\mathbf{T}' - \mathbf{F}^{*\prime}). \tag{12}$$

To complete the general description of the model, it is necessary to introduce the power $\mathscr{D}$ expended in the dissipative mechanisms:

$$\mathscr{D} = \mathbf{T}\cdot\dot{\mathbf{E}}_{\mathrm{n}}^{*} + \mathbf{T}\cdot\dot{\mathbf{E}}_{\mathrm{t}}^{*}. \tag{13}$$

The first term of the sum in Eq. (13) can be rewritten making use of the identity:

$$\mathbf{T}\cdot\dot{\mathbf{E}}_{\mathrm{n}}^{*} = (\mathbf{T} - \mathbf{P}^{*})\cdot\dot{\mathbf{E}}_{\mathrm{n}}^{*} + \mathbf{P}^{*}\cdot\dot{\mathbf{E}}_{\mathrm{n}}^{*}, \tag{14}$$

and noting that Eq. (11a) can be used to obtain:

$$(\mathbf{T} - \mathbf{P}^{*})\cdot\dot{\mathbf{E}}_{\mathrm{n}}^{*} = \frac{3}{2}c_{\mathrm{n}}\alpha^{2}(\mathbf{T} - \mathbf{P}^{*})\cdot\mathbf{H}_{\mathrm{n}}(\mathbf{T} - \mathbf{P}^{*})\dot{\alpha} + \frac{1}{2}c_{\mathrm{n}}\overbrace{\alpha^{3}(\mathbf{T} - \mathbf{P}^{*})\cdot\mathbf{H}_{\mathrm{n}}(\mathbf{T} - \mathbf{P}^{*})}^{\bullet}. \tag{15}$$

The second term on the right-hand side of Eq. (15) represents the recoverable power of the mechanism during the deformation process and is vanishing in a closed process, so that the power expended in the opening mechanisms gets the following form:

$$\mathbf{T}\cdot\dot{\mathbf{E}}_{\mathrm{n}}^{*} = \mathbf{P}^{*}\cdot\dot{\mathbf{E}}_{\mathrm{n}}^{*} + \tfrac{3}{2}c_{\mathrm{n}}\alpha^{2}[(\mathbf{T} - \mathbf{P}^{*})\cdot\mathbf{H}_{\mathrm{n}}(\mathbf{T} - \mathbf{P}^{*})]\dot{\alpha}. \tag{16}$$

Analogous considerations allow the computation of the power expended in the sliding inelastic mechanisms, obtaining the general form:

$$\mathscr{D} = \mathbf{P}^{*}\cdot\dot{\mathbf{E}}_{\mathrm{n}}^{*} + \mathbf{F}^{*\prime}\cdot\dot{\mathbf{E}}_{\mathrm{t}}^{*} + \mathrm{Y}\dot{\alpha} \tag{17}$$

in which the variable

$$\begin{aligned}\mathrm{Y} &= \tfrac{3}{2}\alpha^{2}\left[c_{\mathrm{n}}(\mathbf{T} - \mathbf{P}^{*})\cdot\mathbf{H}_{\mathrm{n}}(\mathbf{T} - \mathbf{P}^{*}) + c_{\mathrm{t}}\left|\mathbf{T}' - \mathbf{F}^{*\prime}\right|^{2}\right]\\ &= \tfrac{3}{10}\alpha^{2}\left[2c_{\mathrm{n}}|\mathbf{T} - \mathbf{P}^{*}|^{2} + c_{\mathrm{n}}\,\mathrm{tr}^{2}(\mathbf{T} - \mathbf{P}^{*}) + 5c_{\mathrm{t}}\left|\mathbf{T}' - \mathbf{F}^{*\prime}\right|^{2}\right]\end{aligned} \tag{18}$$

is introduced and represents the energy release rate corresponding to the infinitesimal damage evolution $\dot{\alpha}$. Eq. (17) points out the tensors $\mathbf{P}^{*}$ and $\mathbf{F}^{*\prime}$ and the scalar Y as variables conjugated to the strains $\mathbf{E}_{\mathrm{n}}^{*}$ and $\mathbf{E}_{\mathrm{t}}^{*}$ and to the damage variable α.

3. Evolution equations

The different response under tensile and compressive stresses is considered in this section both in terms of evolution equations of the internal variables and the stress–strain relations and in terms of the limit states for the elastic response and for the limit strength.

3.1. Open microcracks

In the case of open cracks on every orientation ($p = 0\ \forall \mathbf{n}$) the stress field is a tensile one ($\mathbf{P}^* = \mathbf{0}$) and no frictional sliding ($\mathbf{F}^{*\prime} = \mathbf{0}$) can be expected. Following an $\mathscr{R}$-curve approach, propagation ($\dot{\alpha} > 0$) is assumed to take place when the strain energy release Y equals the damage resistance function $\mathscr{R}(\alpha)$ (Ouyang et al., 1990; Krajcinovic, 1996). The admissible states are therefore characterised by the following condition:

$$\Phi_{\mathrm{d}} = \mathrm{Y}(\alpha, \mathbf{T}) - \mathscr{R}(\alpha) \leqslant 0, \tag{19}$$

where $\mathscr{R}(\alpha)$ is a monotonically increasing function of $\alpha \in (1, \infty)$, with $\mathscr{R}(\alpha = 1) = 0$, that represents the overall measure of the material fracture toughness (Ouyang et al., 1990), in the sense of an average value over all the orientations $\mathbf{n}$.

When condition (19) holds as a strict inequality, the resistance function overcomes the strain energy release and no damage evolution can take place. A limit state is given by Eq. (19) holding as an equality; in this case the resistance $\mathscr{R}(\alpha)$ is equal to $\mathrm{Y}(\alpha, \mathbf{T})$ and two different evolutions are possible in the loading process: (a) elastic unloading ($\dot{\Phi}_{\mathrm{d}} < 0$) that is again described by Eq. (19) as an inequality and (b) damage evolution ($\dot{\Phi}_{\mathrm{d}} = 0$ and $\dot{\alpha} > 0$) which keeps active the limit condition $\Phi_{\mathrm{d}} = 0$. In both cases the damage rate is obtained as the solution of the LCP:

$$\dot{\Phi}_{\mathrm{d}} \leqslant 0, \quad \dot{\alpha} \geqslant 0, \quad \dot{\Phi}_{\mathrm{d}}\dot{\alpha} = 0. \tag{20}$$

Recalling Eqs. (18) and (19), the first term of Eq. (20) is re-written in the form:

$$\dot{\Phi}_{\mathrm{d}} = \dot{s} - d\dot{\alpha} = 3\alpha^2[c_{\mathrm{n}}\dot{\mathbf{T}} \cdot \mathbf{H}_{\mathrm{n}}\mathbf{T} + c_{\mathrm{t}}\dot{\mathbf{T}}' \cdot \mathbf{T}'] - \frac{\partial(\mathscr{R} - \mathrm{Y})}{\partial\alpha}\dot{\alpha} \leqslant 0. \tag{21}$$

An interpretation of Eqs. (20) and (21) is given in Fig. 1 by analysing the different cases corresponding to the evolution from a given status and depending on the damage resistance function $\mathscr{R}(\alpha)$.

(I) *Stable response* $d > 0$: In this case $\partial\mathscr{R}/\partial\alpha > \partial\mathrm{Y}/\partial\alpha$ and crack propagation is stable and the solution is unique:

$$\dot{s} > 0 \ \Rightarrow \ \dot{\alpha} = \frac{\dot{s}}{d} > 0 \ \Rightarrow \ \text{damage evolution},$$

$$\dot{s} < 0 \ \Rightarrow \ \dot{\alpha} = 0 \ \Rightarrow \ \text{elastic unloading}.$$

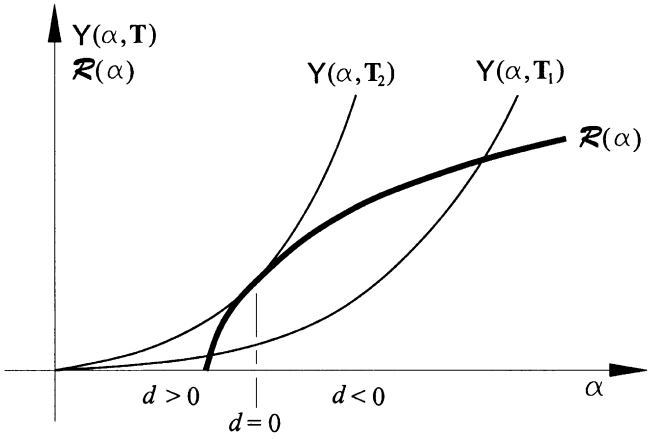

Fig. 1. Geometric representation of the strain energy release $\mathrm{Y}(\alpha, \mathbf{T})$ and resistance $\mathscr{R}(\alpha)$ functions.

(II) *Strain softening* $d < 0$: Crack propagation turns to be unstable and stress states with $\dot{s} > 0$ are not admissible. In the remaining cases $\dot{s} \leqslant 0$ the solution is not unique, since both unloading and damage evolution are possible:

$$\dot{s} \leqslant 0 \;\Rightarrow\; \dot{\alpha} = \frac{\dot{s}}{d} > 0 \;\Rightarrow\; \text{damage evolution},$$

$$\dot{s} \leqslant 0 \;\Rightarrow\; \dot{\alpha} = 0 \;\Rightarrow\; \text{elastic unloading}.$$

(III) *Limit point* $d = 0$: The separation between the two stages of stable and unstable damage evolution defines the limit point for s, and corresponds to the peak load when the strain energy release equals the material resistance and the damage variable α attains a critical value α_c.

The three preceding cases are given a geometric representation in Fig. 2, in terms of a stress damage and a stress–strain curve for a strain softening material, giving a physical explanation to problem (20).

As an example, let us consider the case of uniaxial tensile stress represented by the tensor $\mathbf{T} = \sigma(\mathbf{e} \otimes \mathbf{e})$. At the peak load the damage variable gets the critical value α_c and must satisfy all the three conditions:

$$\Phi_d = \tfrac{1}{10}\alpha_c^2(9c_n + 10c_t)\sigma^2 - \mathscr{R}(\alpha) = 0, \tag{22a}$$

$$\dot{\Phi}_d = \dot{s} - d\dot{\alpha} = \tfrac{1}{5}\alpha_c^2(9c_n + 10c_t)\sigma\dot{\sigma} - \left[\mathscr{R}'(\alpha_c) - \tfrac{1}{5}\alpha_c(9c_n + 10c_t)\sigma^2\right]\dot{\alpha}_c = 0, \tag{22b}$$

$$d = \mathscr{R}'(\alpha_c) - \tfrac{1}{5}\alpha_c(9c_n + 10c_t)\sigma^2 = 0, \tag{22c}$$

where $\mathscr{R}'(\alpha_c) = (\partial\mathscr{R}/\partial\alpha)_{\alpha=\alpha_c}$.

The comparison of Eqs. (22a) and (22c) shows that, at the critical condition corresponding to the peak load, the damage α_c must satisfy the following equation:

$$\mathscr{R}'(\alpha_c) = \frac{2\mathscr{R}(\alpha_c)}{\alpha_c} \tag{23}$$

from which the tensile uniaxial strength is deduced:

$$\sigma_T = \sqrt{\frac{10\mathscr{R}(\alpha_c)}{\alpha_c^2(9c_n + 10c_t)}}. \tag{24}$$

Condition (23) holds also for a generic triaxial stress state satisfying conditions $\mathbf{P} = \mathbf{0}$ and $\mathbf{F}^{*\prime} = \mathbf{0}$, so that, in the frame of the present model, it turns out to be a general characteristic of the tensile critical stress

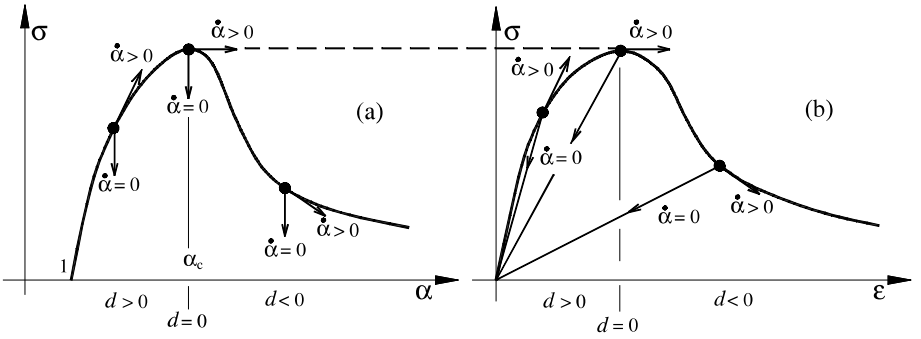

Fig. 2. Geometric representation of problem (20): (a) stress-damage and (b) stress–strain diagrams.

field. For a generic triaxial tensile loading, the critical condition corresponding to the peak strength is obtained imposing $\Phi_d = \dot{\Phi}_d = d = 0$ and depends on the stress state:

$$(2+5\rho)|\mathbf{T}|^2 + 3(3-5\rho)\mathrm{p}^2 = (2+5\rho)\left|\mathbf{T}'\right|^2 + 15\mathrm{p}^2 = \frac{10}{3c_n\alpha_c^2}\mathscr{R}(\alpha_c), \tag{25}$$

where p is the hydrostatic stress component and ρ represents the ratio between the tangential and normal compliances $\rho = c_t/c_n$.

The biaxial tensile strength σ_{TT} and the triaxial one σ_{TTT} are then obtained, respectively:

$$\sigma_{TT} = \sqrt{\frac{5\mathscr{R}(\alpha_c)}{c_n\alpha_c^2(12+5\rho)}} = \sqrt{\frac{(9+10\rho)}{(24+10\rho)}}\sigma_T, \tag{26a}$$

$$\sigma_{TTT} = \sqrt{\frac{2\mathscr{R}(\alpha_c)}{9c_n\alpha_c^2}} = \sqrt{\frac{9+10\rho}{45}}\sigma_T. \tag{26b}$$

3.2. Partially closed or closed microcracks

When a compressive stress acts on some orientation **n**, the limit damage condition $\Phi_d = Y(\alpha, \mathbf{T}, \mathbf{P}^*, \mathbf{F}^*) - \mathscr{R}(\alpha) \leqslant 0$, must be considered simultaneously with a sliding rule related to contact and frictional tractions. In this case tensor $\mathbf{P}^*$ does not vanish and $\mathrm{tr}\,\mathbf{P}^* < 0$ is proportional to the average compressive stress on the damage planes. As a consequence, frictional sliding on compressed crack faces can take place according to a limit condition depending on the frictional tractions **f** and on the normal stress σ. In the frame of the present model, the limit condition is given in terms of the global friction tensor $\mathbf{F}^{*\prime}$ and the average compressive stress $\mathrm{tr}\,\mathbf{P}^*$. In fact, the overall friction limit state, ruling the evolution of the overall sliding, should take into account on the average the local Coulomb frictional condition $\Phi_s = |\mathbf{f}| + \mu p \leqslant 0$ related to the **n**-oriented crack plane. Moreover, the overall sliding rule has to be defined in accordance with the local sliding rule $\dot{\boldsymbol{\gamma}} = \mathbf{v}\dot{\lambda}(\dot{\lambda} \geqslant 0)$, being the unit sliding vector $\mathbf{v} = \mathbf{f}/|\mathbf{f}|$, and without considering any dilatancy effect ($\dot{\varepsilon} = 0$). Since in the present analysis the description of the contact and frictional tractions is provided only in average form through the tensor $\mathbf{P}^*$ and $\mathbf{F}^{*\prime}$ respectively, the limit sliding condition is assumed as follows:

$$\Phi_s(\mathbf{F}^{*\prime}, \mathbf{P}^*) = f(|\mathbf{F}^{*\prime}|) + g(\mathrm{tr}\,\mathbf{P}^*) \leqslant 0, \quad g(0) = 0,\ f(0) = 0,\ f(\bullet) \geqslant 0. \tag{27}$$

This form of the sliding limit condition allows the representation of frictional dissipative mechanisms under compressive stress states only; for tensile dominating stress states ($\mathrm{tr}\,\mathbf{P}^* = \mathbf{0}$) Eq. (27) implies $\mathbf{F}^{*\prime} = \mathbf{0}$, so that damage can be modelled in the standard form of Section 3.1.

The admissibility condition (27) needs a flow rule to be defined providing the traceless strain increment:

$$\dot{\mathbf{E}}_t^* = \mathbf{V}\dot{\lambda}, \quad \dot{\lambda} \geqslant 0, \tag{28a, b}$$

where

$$\mathbf{V} = |x|^{-1}\frac{\partial\Phi_s}{\partial\mathbf{F}^{*\prime}} \tag{28c}$$

and $\dot{\lambda}$ is a non-negative multiplier. Thus, when compression acts on some plane, frictional and damage limits must be considered:

$$\Phi_d \leqslant 0, \quad \Phi_s \leqslant 0, \tag{29a, b}$$

while damage and flow rates at the limit states $\Phi_d = 0$ and $\Phi_s = 0$, respectively, are given as solutions of the LCPs:

$$\dot{\Phi}_d \leqslant 0, \quad \dot{\alpha} \geqslant 0, \quad \dot{\Phi}_d \dot{\alpha} = 0, \tag{30a–c}$$

$$\dot{\Phi}_s \leqslant 0, \quad \dot{\lambda} \geqslant 0, \quad \dot{\Phi}_s \dot{\lambda} = 0, \tag{30d–f}$$

providing the general expressions of the inelastic strain rates:

$$\dot{\mathbf{E}}_n^* = c_n \alpha^3 \mathbf{H}_n(\dot{\mathbf{T}} - \dot{\mathbf{P}}^*) + 3c_n \alpha^2 \mathbf{H}_n(\mathbf{T} - \mathbf{P}^*)\dot{\alpha}, \qquad \dot{\mathbf{E}}_t^* = \mathbf{V}\dot{\lambda}. \tag{31a, b}$$

The choice of functions Φ_s needs to take into account the influence of the deviatoric and hydrostatic part of the average friction internal forces. To this end, different choices can be made based on the similarities with limit strength domains, ranging from the simple Drucker–Prager criterion (Drucker and Prager, 1952) to the more elaborate five parameter model by Etse and Willam (1995), taking into account the effect of the intermediate principal stress.

The simplest choice is based on a global limit function analogous to the Drucker–Prager limit state in the case of vanishing cohesion:

$$\Phi_s = \left|\mathbf{F}^{*\prime}\right| + \mu \operatorname{tr} \mathbf{P}^* \leqslant 0, \tag{32}$$

where the parameter μ plays the role of a global friction coefficient. Here $|\mathbf{F}^{*\prime}|$ is assumed as a global measure of the friction tensor and therefore makes the sliding condition (32) to represent an isotropic limit state.

Making use of Eq. (11b), the limit sliding condition (32) takes the form:

$$\Phi_s = \left|\mathbf{T}' - \frac{1}{c_t \alpha^3}\mathbf{E}_t^*\right| + \mu \operatorname{tr} \mathbf{P}^* \leqslant 0, \tag{33}$$

moreover, since in this case $\mathbf{P}^* \neq \mathbf{0}$, condition (19) becomes

$$\Phi_d = \frac{3}{2} c_n \alpha^2 (\mathbf{T} - \mathbf{P}^*) \cdot \mathbf{H}_n(\mathbf{T} - \mathbf{P}^*) + \frac{3}{2c_t \alpha^4}\left|\mathbf{E}_t^*\right|^2 - \mathscr{R}(\alpha) \leqslant 0, \tag{34}$$

and from Eqs. (28c), (32) and (11b) it follows:

$$\mathbf{V} = \frac{\mathbf{F}^{*\prime}}{|\mathbf{F}^{*\prime}|} = \left(\mathbf{T}' - \frac{1}{c_t \alpha^3}\mathbf{E}_t^*\right) \Big/ \left|\mathbf{T}' - \frac{1}{c_t \alpha^3}\mathbf{E}_t^*\right|. \tag{35}$$

According to the actual values of the variables at the initial state of the load step and to the applied stress rate $\dot{\mathbf{T}}$, different evolutions, characterised by damage and/or sliding mechanisms, can be distinguished as follows.

(1) The initial state is characterised by negative values of the limit functions $\Phi_d < 0$ and $\Phi_s < 0$, so that neither sliding nor damage growth take place; the strain rate is then

$$\dot{\mathbf{E}}_n^* = c_n \alpha^3 \mathbf{H}_n(\dot{\mathbf{T}} - \dot{\mathbf{P}}^*), \quad \dot{\mathbf{E}}_t^* = \mathbf{0}, \qquad \alpha \in [0; 1), \tag{36a, b}$$

where

$$\dot{\mathbf{P}}^* = \mathbf{H}_n^{-1} \frac{3}{2\pi} \int_{\Omega^-} \dot{p}\mathbf{n} \otimes \mathbf{n} \, d\Omega. \tag{37}$$

(2) The initial state is a sliding limit one $\Phi_s = 0$ but $\Phi_d < 0$, so that no damage evolution takes place ($\dot{\alpha} = 0$) and the sliding rate $\dot{\lambda}$ is obtained as solution of the LCP:

$$\dot{\Phi}_s = -\frac{1}{c_t \alpha^3}\dot{\lambda} + \dot{t}_s \leqslant 0, \tag{38a}$$

$$\dot{\lambda} \geqslant 0, \quad \dot{\Phi}_s \dot{\lambda} = 0, \tag{38b, c}$$

where

$$\dot{t}_s = \mathbf{V} \cdot \dot{\mathbf{T}}' + \mu \operatorname{tr}(\dot{\mathbf{P}}^*). \tag{39}$$

Two evolutions are possible:

(a) *locking of sliding mechanisms*

$$\dot{t}_s \leqslant 0 \;\Rightarrow\; \dot{\lambda} = 0, \tag{40a, b}$$

(b) *sliding without damage*

$$\dot{t}_s > 0 \;\Rightarrow\; \dot{\lambda} = c_t \alpha^3 \dot{t}_s. \tag{40c, d}$$

(3) When the initial state is a limit damage state $\Phi_d = 0$ with no sliding allowed ($\Phi_s < 0$), only the strain rate $\dot{\mathbf{E}}_n^*$ is obtained. In this case, that is characteristic of states with a relevant number of opened crack planes ($\mathbf{H}_n \mathbf{T} \neq \mathbf{P}^*$), the rate $\dot{\alpha}$ is obtained as the solution of the LCP:

$$\dot{\Phi}_d = \dot{t}_d - d\dot{\alpha} \leqslant 0, \quad \dot{\alpha} \geqslant 0, \quad \dot{\Phi}_d \dot{\alpha} = 0, \tag{41a–c}$$

where

$$d = \mathscr{R}'(\alpha) + \frac{6}{c_t \alpha^5}\left|\mathbf{E}_t^*\right|^2 - 3c_n \alpha (\mathbf{T} - \mathbf{P}^*) \cdot \mathbf{H}_n (\mathbf{T} - \mathbf{P}^*), \tag{42}$$

$$\dot{t}_d = 3c_n \alpha^2 (\mathbf{T} - \mathbf{P}^*) \cdot \mathbf{H}_n (\dot{\mathbf{T}} - \dot{\mathbf{P}}^*). \tag{43}$$

Different evolutions are possible, depending on the sign of d and on the rate $\dot{t}_d$. In analogy to the cases considered in Section 3.1 (open microcracks) the response can be distinguished as follows:

(a) *unloading*

$$\dot{t}_d \leqslant 0 \quad \text{and } d \neq 0 \;\Rightarrow\; \dot{\alpha} = 0, \tag{44}$$

(b) *damage without sliding*

$$\dot{\alpha} = \frac{\dot{t}_d}{d} > 0, \tag{45}$$

which is possible either during the *hardening* phase $\dot{t}_d > 0$ and $d > 0$, or in the *softening* phase $\dot{t}_d < 0$ and $d < 0$. It is worthwhile noting that a positive stress increment, leading to $\dot{t}_d > 0$, cannot take place when the peak load has been exceeded ($d < 0$).

The critical condition defined by a vanishing value for d represents a limit state, depending on the inelastic sliding strain $\mathbf{E}_t^*$, that marks the transition between the stable and the unstable model response under stress control. When proportional loading cases are considered, starting from an unloaded initial state where no inelastic tangential strain is present $\mathbf{E}_t^* = \mathbf{0}$, the condition $d = 0$ together with the limit condition (34) and (24) provide the limit strength criterion:

$$(\mathbf{T} - \mathbf{P}^*) \cdot \mathbf{H}_n (\mathbf{T} - \mathbf{P}^*) = \frac{9 + 10\rho}{15}\sigma_T^2. \tag{46}$$

(4) The two simultaneous conditions $\Phi_s = \Phi_d = 0$ are attained at the initial state, so that the evolution of the internal variables can be obtained as the solution of the LCP:

$$\begin{Bmatrix} \dot{\Phi}_d \\ \dot{\Phi}_s \end{Bmatrix} = \begin{bmatrix} a_{11} & a_{12} \\ a_{21} & a_{22} \end{bmatrix} \begin{Bmatrix} \dot{\alpha} \\ \dot{\lambda} \end{Bmatrix} + \begin{Bmatrix} \dot{t}_d \\ \dot{t}_s \end{Bmatrix} \leqslant \mathbf{0}, \tag{47a}$$

$$\begin{Bmatrix} \dot{\alpha} \\ \dot{\lambda} \end{Bmatrix} \geqslant \mathbf{0}, \qquad \{ \dot{\Phi}_d \quad \dot{\Phi}_s \} \begin{Bmatrix} \dot{\alpha} \\ \dot{\lambda} \end{Bmatrix} = 0, \tag{47b, c}$$

where

$$a_{11} = -d, \tag{48a}$$

$$a_{12} = a_{21} = \frac{3}{c_t \alpha^4} \mathbf{V} \cdot \mathbf{E}_t^*, \tag{48b}$$

$$a_{22} = -\frac{1}{c_t \alpha^3}, \tag{48c}$$

and $\dot{t}_s$, d and $\dot{t}_d$ are defined, respectively, in Eqs. (39), (42) and (43).

The solution of the LCP (47a) and (47b,c) is unique as far as the matrix $\mathbf{A}$ is a P-matrix (Cottle et al., 1992) which requires that

$$d > 0, \quad \det \mathbf{A} = \frac{1}{c_t \alpha^3} d - \frac{9}{c_t^2 \alpha^8} \left| \mathbf{E}_t^* \right|^2 > 0, \tag{49a, b}$$

the latter being the more restrictive. Four solutions are possible according to these conditions and to the rates $\dot{t}_s$ and $\dot{t}_d$. In particular, three of them have already been given in the previous subsections ((1) neither sliding nor damage evolution; (2) sliding without damage; and (3) damage without sliding). The rates of the internal variables in the fourth case, characterised by sliding and damage coupling, are obtained by Eq. (47a) when holding as a strict equality $\dot{\Phi}_s = \dot{\Phi}_d = 0$.

On the other hand, if condition $\det \mathbf{A} < 0$ occurs, multiple solutions are obtained for prescribed rates $\dot{t}_s$ and $\dot{t}_d$, distinguished between damage-sliding evolution and locking with damage arrest. In this case it follows that the model responses to prescribed stress rates are distinguished by different strain rates.

To clarify this aspect, proportional loading paths are considered. At the beginning of the load process the limit conditions $\Phi_s = \Phi_d = 0$ are attained and the subsequent load steps are selected in order to maintain such limit stress states active. At the onset of sliding ($\mathbf{E}_t^* = \mathbf{0}, \alpha = 1$), because of condition (33) and definition (35), one obtains that tensors $\mathbf{V}$, $\mathbf{F}^{*\prime}$ and $\mathbf{T}'$ are coaxial; therefore in the subsequent load steps we can assume $\mathbf{E}_t^* = \mathbf{V}\dot{\lambda}$ during the deformation process, so that $\mathbf{V} \cdot \mathbf{E}_t^* = \left| \mathbf{E}_t^* \right|$. Subsequently the condition $\det \mathbf{A} = 0$ at the limit state becomes

$$\mathscr{R}'(\alpha_c) - \frac{3}{c_t \alpha_c^5} \left| \mathbf{E}_t^* \right|^2 - 3 c_n \alpha_c (\mathbf{T} - \mathbf{P}^*) \cdot \mathbf{H}_n (\mathbf{T} - \mathbf{P}^*) = 0, \tag{50}$$

where α_c stands for the damage value at the critical state. By comparing Eq. (50) with condition $\Phi_d = 0$ imposed to Eq. (34), one obtains Eq. (23) that provides, once the toughness function $\mathscr{R}(\bullet)$ is selected, the damage entity α_c at the critical state, independent of the stressing mode. Moreover, from condition (32) at the limit state, it follows:

$$\left| \mathbf{F}^{*\prime} \right| = -\mu \operatorname{tr} \mathbf{P}^*, \tag{51}$$

and therefore from the previous considerations:

$$\mathbf{F}^{*\prime} = -\mu \operatorname{tr}\mathbf{P}^* \frac{\mathbf{T}'}{|\mathbf{T}'|}. \tag{52}$$

Substituting Eq. (52) into Eq. (11b), the inelastic strain is obtained:

$$\mathbf{E}_{\mathrm{t}}^* = c_{\mathrm{t}}\alpha^3 \left(\mathbf{T}' + \mu \operatorname{tr}\mathbf{P}^* \frac{\mathbf{T}'}{|\mathbf{T}'|} \right). \tag{53}$$

The critical state $\det \mathbf{A} = 0$ can be formulated in terms of the applied stress $\mathbf{T}$ by substituting in condition (34), holding as a strict equality, the critical damage α_{c} and the inelastic strain tensor $\mathbf{E}_{\mathrm{t}}^*$ by Eq. (53) as follows:

$$\tfrac{2}{5}|\mathbf{T} - \mathbf{P}^*|^2 + \tfrac{1}{5}(3\mathrm{p} - \operatorname{tr}\mathbf{P}^*)^2 + \rho\left(|\mathbf{T}'| + \mu \operatorname{tr}\mathbf{P}^*\right)^2 = 3\sigma_{\mathrm{TTT}}^2. \tag{54}$$

When compressive normal stresses are active on each plane it follows from definitions (4), (7c) and (10a) that $\mathbf{P}^* = \mathbf{T}$ and the critical condition (54) takes the form of the criterion of Drucker–Prager (1952) as follows:

$$|\mathbf{T}'| + 3\mu\mathrm{p} = \sqrt{\frac{3}{\rho}}\sigma_{\mathrm{TTT}} = \frac{1}{\sqrt{3}}\sqrt{\frac{2\mathscr{R}(\alpha_{\mathrm{c}})}{c_{\mathrm{t}}\alpha_{\mathrm{c}}^2}}. \tag{55}$$

In the pre-peak phase the stress intensity is controlled by an increasing scalar variable, so that the rates $\dot{\imath}_{\mathrm{s}}$ and $\dot{\imath}_{\mathrm{d}}$ are proportional one to the other. By discussing the solutions of the LCP (47a) and (47b,c) in terms of the data $\dot{\imath}_{\mathrm{s}}$ and $\dot{\imath}_{\mathrm{d}}$, it may be argued that the transition from positive values of $\det \mathbf{A}$ to negative ones is characterised by a maximum for the load control variable, so that conditions (54) and (55) can be assumed as limit strength conditions for the model under dominant compressive stresses ($\operatorname{tr}\mathbf{P}^* < 0$).

By the limit state defined by equation (54) the uniaxial σ_{C} and biaxial σ_{CC} compressive strengths as functions of the model parameters are obtained as follows:

$$\sigma_{\mathrm{C}} = -\sqrt{\frac{3}{\rho}}\frac{1}{\sqrt{2/3} - \mu}\sigma_{\mathrm{TTT}}, \tag{56a}$$

$$\sigma_{\mathrm{CC}} = -\sqrt{\frac{3}{\rho}}\frac{1}{\sqrt{2/3} - 2\mu}\sigma_{\mathrm{TTT}} \tag{56b}$$

from which an upper bound for the friction coefficient $\mu < \sqrt{1/6}$ is established. Finally, it is worth noting that assumption (32) makes the model unable to predict the triaxial compressive strength, in partial accord with the mechanical response exhibited by brittle concrete-like materials.

4. Model response

In order to provide a comprehensive description of the proposed model, the stress–strain response to significant load paths and limit strength domains for bi and triaxial stress states needs to be derived. In this paragraph the stress–strain response for uniaxial and biaxial stress states is discussed and extended to the post-peak phase in order to provide a complete description of the model response; comparison to experimental data is given up to the peak load, which is the limit for homogeneous damage phenomena and, therefore, the limit of validity of the proposed model.

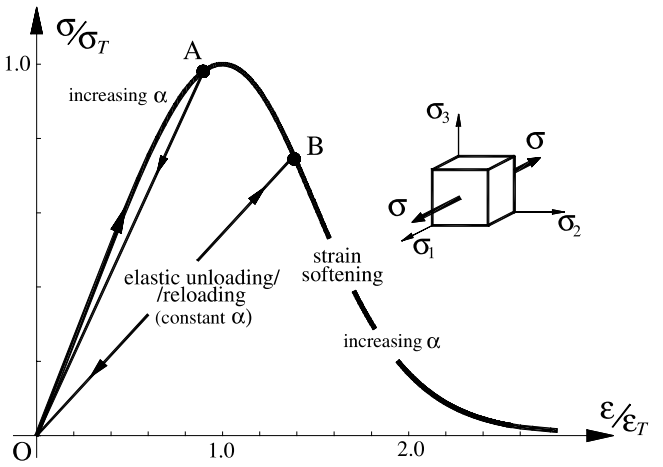

Fig. 3. Model response to uniaxial tensile stress ($c_n = 5 \times 10^{-3}$ MPa^{-1}, $\rho = 0.05$, $E = 3 \times 10^4$ MPa, $\mu = 0.2$, $\mathscr{R}(\alpha) = a(\alpha - 1)^{1/2}/(\alpha^8 - b)^{-1/2}$ ($a = 0.1$ MPa, $b = 1 \times 10^{-7}$)).

Let us first consider the model response to uniaxial tensile stress states. In this case it follows, from Eqs. (2a), (2b) and (4–7), that $\mathbf{P}^* = \mathbf{0}$ and $\mathbf{F}^{*\prime} = \mathbf{0}$, since every crack plane is open and the damage variable α grows according to the admissibility condition (19).

The uniaxial tensile response is represented in the diagram of Fig. 3, where ε_T stands for the deformation (strain) corresponding to the critical state (σ_T, α_c), the critical value being given by Eq. (23) once the analytical form of the resistance function $\mathscr{R}$ is assumed (deduced from Ouyang et al. (1990) for Fig. 3).

In the stable phase α increases its value from unity to the critical value α_c; after the peak load is reached the damage variable increases as well, while only in the unloading phase α attains a constant value (no damage increase) and the response is linear elastic. In a further reloading phase the damage variable remains constant up the point at which the unloading phase previously started (points A and B); from this point on it will increase again.

The model allows no permanent strain since the cracks simply close whatever their length and opening (load paths O–A–O and O–B–O). Once the load is completely removed (point O), reloading exhibits the last apparent elastic modulus, that is to say path OA or OB in Fig. 3.

The uniaxial compressive response of the model is shown in Fig. 4 for both the stable and the softening phase. During the loading phase (paths O–A and O–B of Fig. 4a) both tangential sliding on the crack

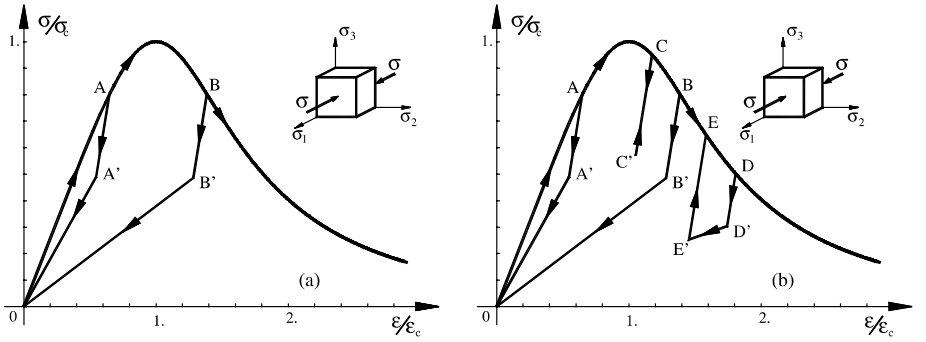

Fig. 4. Model response to uniaxial compressive stress: (a) monotonic loading and complete unloading; (b) partial unloading ($c_n = 5 \times 10^{-3}$ MPa^{-1}, $\rho = 0.05$, $E = 3 \times 10^4$ MPa, $\mu = 0.2$, $\mathscr{R}(\alpha) = a(\alpha - 1)^{1/2}/(\alpha^8 - b)^{-1/2}$ ($a = 0.1$ MPa, $b = 1 \times 10^{-7}$)).

planes and crack growth take place. Since all crack planes are compressed and crack faces are closed, the model response is independent on the parameter c_n. The unloading phase (Fig. 4a), notwithstanding the point (A or B) at which the load is reversed, exhibits two distinct phases: (a) on the paths A–A′ and B–B′ tangential sliding is locked by the frictional stresses on the crack faces, making the response that of the elastic matrix; (b) when the normal stress on crack faces decreases, and friction is reduced, sliding is activated by the elastic unloading of the matrix, so that the overall strain is due to the elastic contribution of the matrix superimposed to the crack sliding contributions (paths A′–O and B′–O) and, again, the recovering of the entire tangential sliding makes the permanent strain to vanish in O. The stress drop from A to A′, or from B to B′, can be evaluated from Eq. (32) holding as a strict equality:

$$\Delta\sigma = 2\mu\tilde{\sigma}\Big/\left(\mu + \sqrt{2/3}\right), \tag{57}$$

where $\tilde{\sigma}$ is the stress value at the unloading point. Finally, the reloading phase is linear because the damage variable remains constant up to the skeleton curve.

Fig. 4b shows the model response for different loading–unloading–reloading paths. Path C–C′ shows that there is no hysteretic dissipation if sliding of the crack faces is not reached due to only a partial relief of the frictional stresses; on the contrary, if tangential sliding is partially recovered (path D–D′–E′) the dissipation effect is due to the frictional sliding of the compressed cracks at constant damage.

In Fig. 5 the uniaxial response of loading–unloading compressive tests with increasing maximum stress level in the stable phase (Maekawa and Okamura, 1983) is shown together with the simulation by the present model assuming a toughness function of the type proposed by Ouyang et al. (1990). A good agreement is found in general, but some points need to be emphasised. The assumption of isotropic damage and a single $\mathscr{R}$-curve damage limit condition do not allow descriptions of the load induced gradual activation of microcracks having different orientations with respect to the load axis. Experimental results point

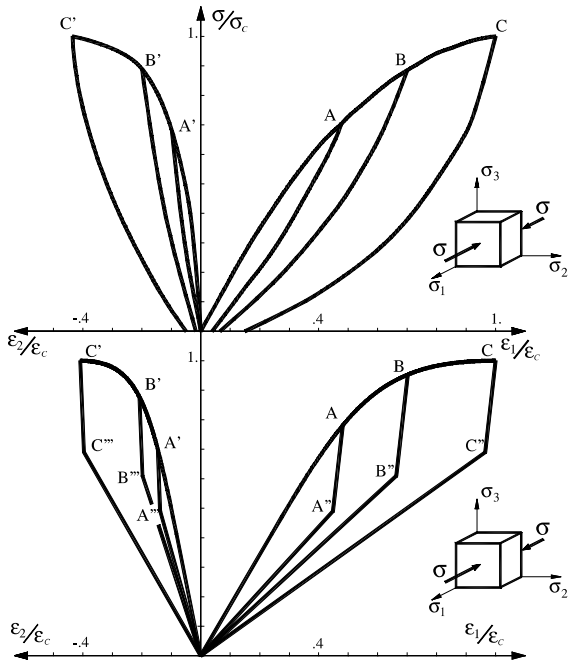

Fig. 5. Uniaxial compressive response: (a) experimental data (Maekawa and Okamura, 1983); (b) theoretical results ($c_n = 5 \times 10^{-3}$ MPa^{-1}, $\rho = 0.05$, $E = 3 \times 10^4$ MPa, $v = 0.30$, $\mu = 0.15$, $\mathscr{R}(\alpha) = r(\alpha - 1)^{1/m}$, ($r = 0.1$ MPa, $m = 2.6$)).

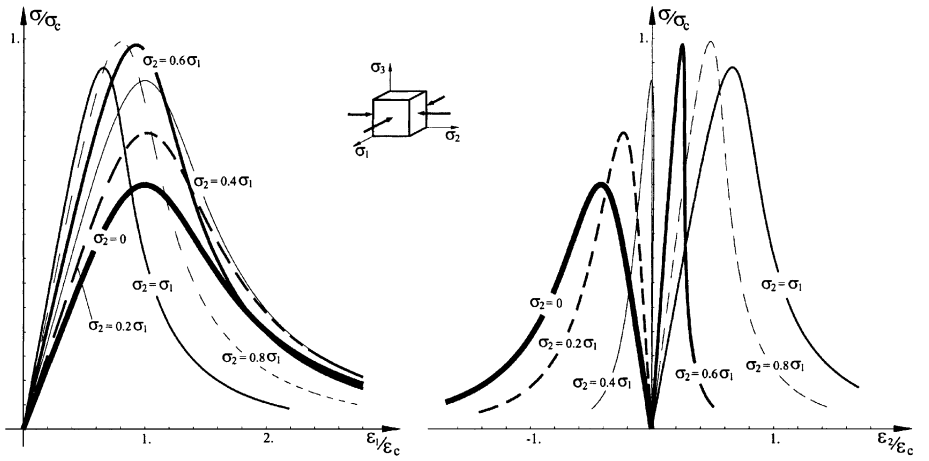

Fig. 6. Response of the model under biaxial compressive stresses: (a) σ_1–ε_1 and (b) σ_1–ε_2 stress–strain response ($c_n = 5 \times 10^{-3}$ MPa^{-1}, $\rho = 0.05$, $E = 3 \times 10^4$ MPa, $\mu = 0.2$, $\mathscr{R}(\alpha) = a(\alpha - 1)^{1/2}/(\alpha^6 - b)^{-1/2}$ ($a = 0.1$ MPa, $b = 1 \times 10^{-7}$)).

out a progressive evolution of the instantaneous compliance in the unloading phase as a consequence of the sliding of the crack faces, while the permanent deformations are due to the presence of sliding mechanisms at some orientation that do not correspond to the frictional model here assumed. On the contrary, in the present model the sliding condition is referred to a single global mechanism excluding progressive sliding.

The model response to biaxial compressive stress states is summarised in Fig. 6 for different ratios σ_2/σ_1. As pointed out by experimental evidences, the biaxial compressive strength is up to 60% higher than the uniaxial one, while transverse compression reduces the limit strain in both the load directions; in the present model this feature strongly depends on the friction coefficient μ. Moreover, the model seems to be able of representing the lateral strain of the material when one stress component prevails over the other and the transition of the lateral strain from expansion to compression for nearly isotropic biaxial stress states.

5. Limit domains for biaxial stress states

On the basis of the results shown in Section 3, the biaxial limit strength domain is here obtained with reference to tensile–tensile, tensile–compressive and compressive–compressive biaxial stress states (indicated as tt, tc and cc respectively). The limit stresses are given in the following as functions of the constants K_1 and K_2 characterising the monotonically increasing stress tensor $\mathbf{T} = \sigma(K_1\mathbf{e}_1 \otimes \mathbf{e}_1 + K_2\mathbf{e}_2 \otimes \mathbf{e}_2)$; besides the model parameters (μ, ρ), two non-dimensional parameters are introduced as $\beta = \sum_i K_i$ and $\psi^2 = \sum_i K_i^2$.

(1) *Tensile–tensile stress states*: $K_1 > 0$, $K_2 > 0$,

$$\sigma_{tt} = \sqrt{\frac{45}{3(2\psi^2 + \beta^2) + 5\rho(3\psi^2 - \beta^2)}}\sigma_{TTT} = \left(\sqrt{\frac{2}{3}} - \mu\right)\sqrt{\frac{15\rho}{3(2\psi^2 + \beta^2) + 5\rho(3\psi^2 - \beta^2)}}\sigma_C, \tag{58}$$

(2) *Tensile–compressive stress states*: $K_1 < 0$, $K_2 > 0$,

$$\sigma_{tc} = \sqrt{\frac{15}{2\Pi^2 + (\beta - \zeta)^2 + 5\rho(\Gamma + \zeta\mu)^2}}\sigma_{TTT} = \left(\sqrt{\frac{2}{3}} - \mu\right)\sqrt{\frac{5\rho}{2\Pi^2 + (\beta - \zeta)^2 + 5\rho(\Gamma + \zeta\mu)^2}}\sigma_C, \tag{59}$$

being

$$\eta^2 = \frac{1}{\sigma^2}\sum_i P_{ii}^2, \quad \varphi^2 = -\frac{1}{\sigma}\sum_i K_i P_{ii}, \quad \zeta = \frac{1}{\sigma}\,\mathrm{tr}\,\mathbf{P}, \quad \Gamma = \sqrt{\psi^2 - \frac{\beta^2}{3}},$$

$$\Pi^2 = \psi^2 + \frac{25}{4}\eta^2 - \frac{7}{4}\zeta^2 + 5\varphi^2 + \zeta\beta,$$

(3) *Compressive–compressive stress states*: $K_1 < 0$, $K_2 < 0$,

$$\sigma_{cc} = \sqrt{\frac{3}{\rho}}\frac{1}{\Gamma - \beta\mu}\sigma_{TTT} = \left(\sqrt{\frac{2}{3}} - \mu\right)\frac{1}{\Gamma - \beta\mu}\sigma_C. \tag{60}$$

Eqs. (58)–(60) give the analytical expression of the limit strength domain for a biaxial stress state and it can be proved that these functions are continuous of class C^2 at the respective connections, which physically represent the uniaxial tensile and compressive strengths. The typical shape of the domain is shown in Fig. 7 and compared with the limit domains obtained from the Rankine, Mohr–Coulomb and Drucker–Prager criteria fitting the uniaxial tensile and compressive strength. It is worthwhile noting that the domain shape depends on the two model parameters only, namely the friction coefficient μ and the ratio ρ.

Figs. 8 and 9 represent a parametric description of the limit domains; in Fig. 8 the model parameter ρ is fixed, while the global friction coefficient is given different values. The friction coefficient μ provides an increase of strength when considering compressive–compressive stress states; being the uniaxial compressive strength σ_C the normalising quantity, also the non-dimensional tensile–compressive and tensile–tensile strengths are indirectly affected by μ.

The alternative parametric representation obtained varying ρ and keeping μ constant is given in Fig. 9; it shows the influence of the ratio ρ only on the stress states characterised by tensile stresses at some orientation. In the frame of the present model, all the cracks are closed in a fully compressive stress state so that the normal compliance coefficient c_n, related to crack openings, play no role in the mechanical response

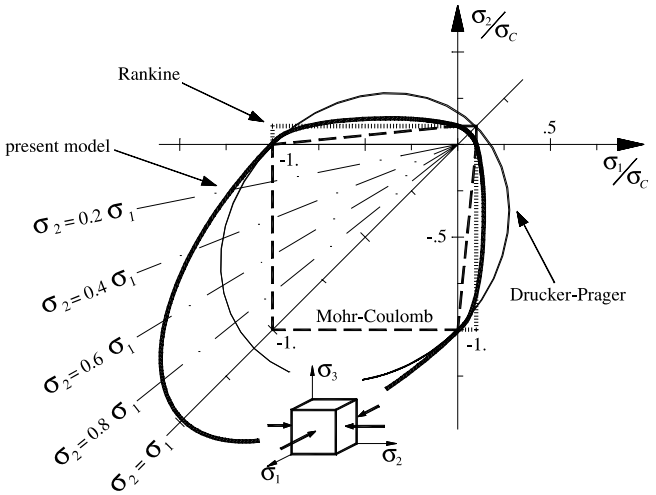

Fig. 7. Biaxial limit strength domain ($\sigma_C/\sigma_T = 10$, $\mu = 0.2$, $\rho = 0.0461$) compared with Rankine, Mohr–Coulomb and Drucker–Prager surfaces.

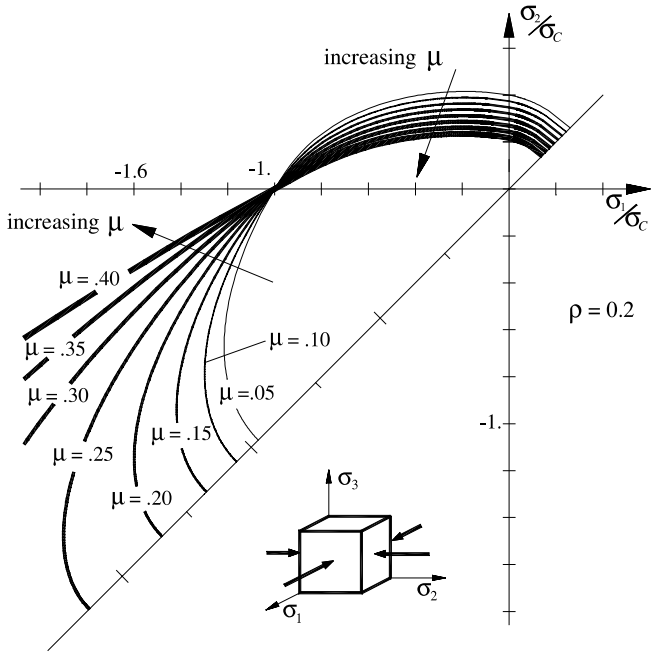

Fig. 8. Biaxial limit domains for fixed ρ and varying μ.

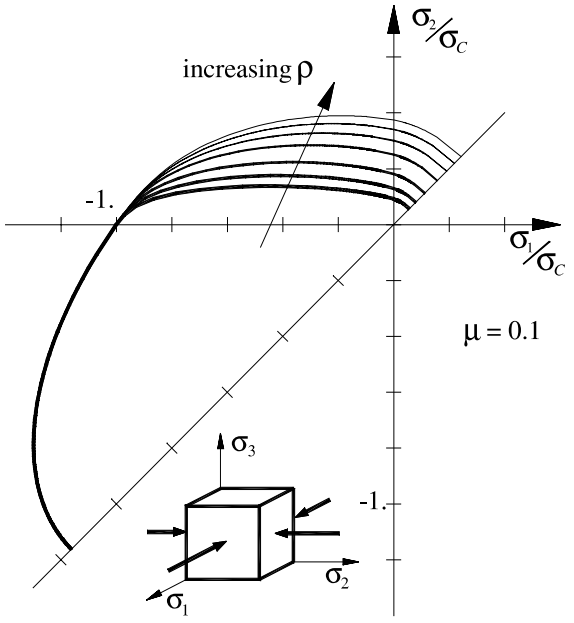

Fig. 9. Biaxial limit domains for varying ρ and fixed μ.

of the model. This is pointed out in Eq. (60) where the limit strength for a general biaxial compressive stress state turns out to be dependent on μ only.

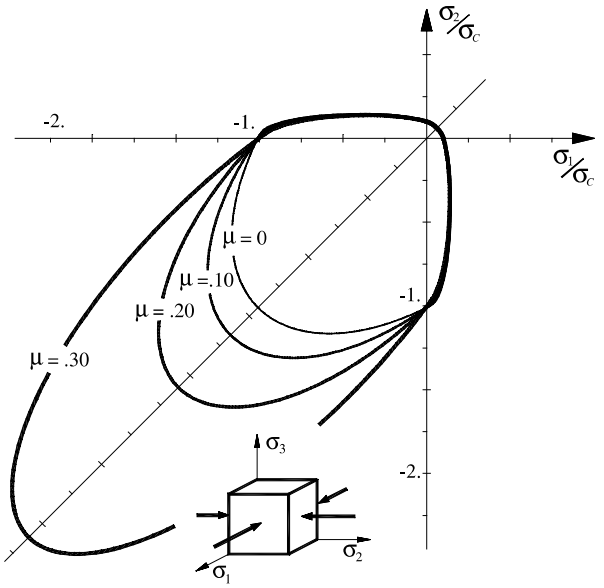

Fig. 10. Biaxial limit domains for varying μ and constant $\rho(\sigma_C/\sigma_T = 10)$.

Once the value of the ratio σ_C/σ_T is given, one of the parameters ρ and μ depends on the other. Assuming the typical ratio $\sigma_C/\sigma_T \cong 10$ representative of brittle materials, the limit domains for various μ are shown in Fig. 10.

The constitutive damage model herein proposed belongs to the class of three parameter models, being defined by ρ, μ and a normalising quantity such as the uniaxial compressive strength. Since limit domains are always referenced to in a non-dimensional stress plane, the parameters that need to be determined are limited only to ρ and μ, that require an identification procedure to be established. When a complete set of experimental data is available, e.g. in terms of principal stress components, the definition of the two parameters can be reduced to an approximation problem. Experimental data can be considered satisfactory if they present number of samples in all the three sectors (tensile–tensile, tensile–compressive and compressive–compressive stresses) large enough to carry out the approximation procedure. While the experimental uncertainty is relatively limited for biaxial compressive stresses, it gets quite high figures when involving tensile stresses, due to the weak tensile resistance of brittle and concrete-like materials and to technical difficulties in reproducing tensile stress states in real specimens (Weigler and Becker, 1961; Kupfer et al., 1969; Liu et al., 1972; Kupfer and Gerstle, 1973; Adenaes et al., 1977; Tasuji et al., 1978); for this reason the fitting of the experimental data involving tensile components is somewhat more troublesome.

For the proposed model to be of practical interest, a simplified identification of the model parameters is needed, based on few material parameters that can be easily obtained from standard experimental tests, such as the uniaxial compressive and the biaxial compressive or uniaxial tensile strength. The proposed model strictly needs only a couple of points to be given, so that we can imagine, in practice, to set up a simplified identification technique that chooses the values for ρ and μ so as to fit exactly the uniaxial and biaxial compressive strengths. In the following part of this section, it will be showed that this simplified technique is usually precise enough to describe the biaxial limit domains.

Fig. 11 shows the biaxial domain obtained through a rigorous approximation technique, bold lines, and by means of a simplified identification approach, dashed lines, for two sets of experimental data on concrete (Weigler and Becker, 1961; Kupfer et al., 1969). It can be seen that a rigorous determination of the

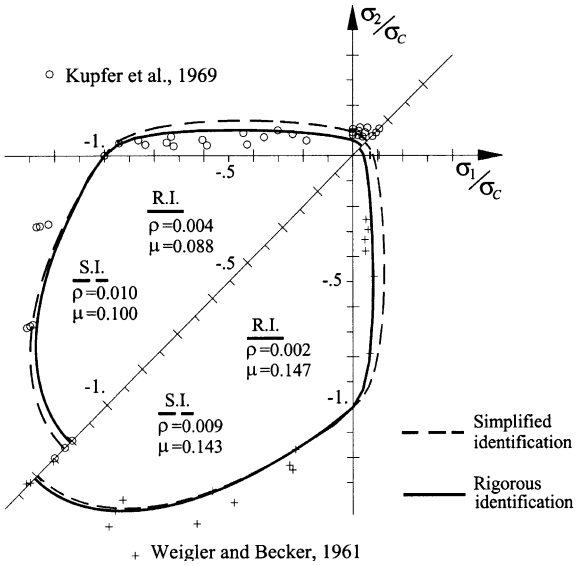

Fig. 11. Biaxial limit domain – data from Weigler and Becker (1961) and Kupfer et al. (1969).

parameters allows a rather good approximation of experimental data in the compression–compression and tension–compression sectors, while material resistance for tensile stress states is significantly underestimated. A rather complementary situation is found in the second case of simplified identification: pure tensile limit stress states are reasonably well approximated, but tensile–compressive ones are quite overestimated. In both cases, anyway, the approximation for pure compressive stresses lies inside the range of the experimental error.

Analogous considerations can be deduced from the comparison with the other experimental data reported in Fig. 12 by Tasuji et al. (1978) and Nelissen (1972) for concrete and mortar, respectively. Fig. 13

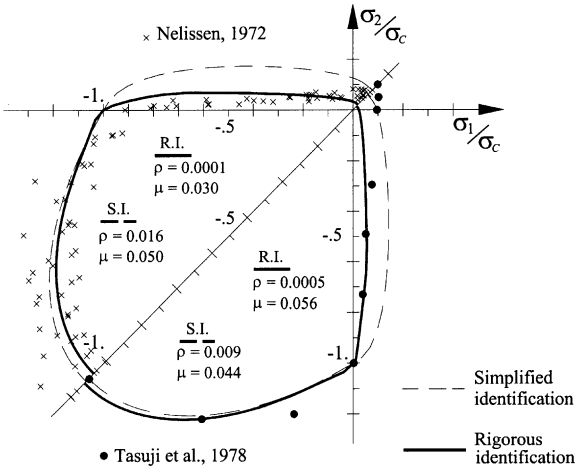

Fig. 12. Biaxial limit domain – data from Tasuji et al. (1978) and Nelissen (1972).

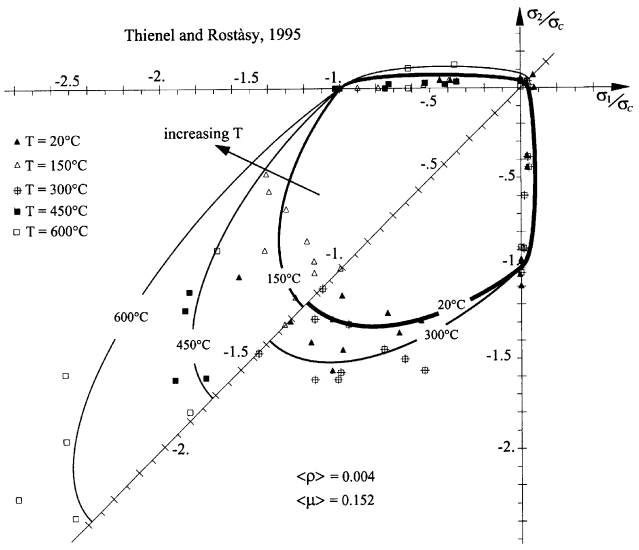

Fig. 13. Biaxial limit domain – data from Thienel and Rostàsy (1995).

presents the limit domains obtained with a rigorous minimisation of the square error for concrete at different temperatures (Thienel and Rostàsy, 1995).

The values attained by the two parameters are limited inside the range $\mu \in (0.04–0.17)$, while $\rho \in (0–0.016)$; the limit domains obtained by a couple of experimental points are characterised by a ratio between the uniaxial compressive and tensile strengths included inside the range (8–12), coherently with experimental evidences.

The proposed model requires that the damage mechanisms of the material can be reduced to crack-like defects propagating in a non-linear brittle matrix. Concrete and mortar meet these requirements, as well as other brittle materials such as cast-iron. Fig. 14 shows the limit curves obtained on the basis of the results

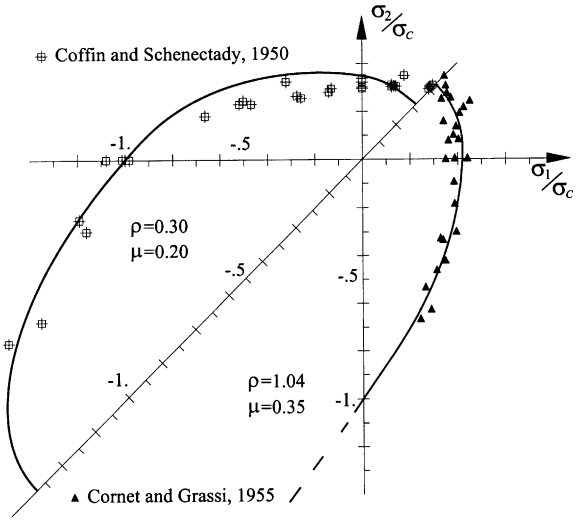

Fig. 14. Biaxial limit domain for cast-iron – data from Coffin and Schenectady (1950) and Cornet and Grassi (1955).

by Coffin and Schenectady (1950), that are again characterised by an overestimation of the tensile–compressive limit stress states; the average fitting, anyway, is quite good. When the limit domain is fitted only in some sectors of the stress plane, such as in the case for the data given in (Cornet and Grassi, 1955) of Fig. 14, the fitting of experimental data is rather good, but the limit function cannot be considered reliable outside the range of values on which the fitting procedure relies.

6. Limit surfaces for triaxial stress states

Triaxial stress states are here represented in terms of the non-dimensional coordinates:

$$\bar{\xi} = \mathrm{tr}\,(\mathbf{T}) \Big/ \left(\sqrt{3}\sigma_{\mathrm{C}}\right) = \sqrt{3}\mathrm{p} \Big/ \sigma_{\mathrm{C}}, \tag{61a}$$

$$\bar{r} = \sqrt{2J_2} \Big/ \sigma_{\mathrm{C}} = \sqrt{3}\tau_{\mathrm{oct}} \Big/ \sigma_{\mathrm{C}}, \tag{61b}$$

$$\theta = 1/3\cos^{-1}\left(\sqrt{27}J_3 \Big/ 2\sqrt{J_2^3}\right), \tag{61c}$$

being J_2 and J_3 the second- and third-order scalar invariants of the deviatoric stress tensor $\mathbf{T}'$, τ_{oct} the octahedral tangential stress and σ_{C} the uniaxial compressive strength. The main features of the limit envelope, a curvilinear triple-symmetric cone, are represented on the tensile ($\theta = 0°$) and compressive ($\theta = 60°$) meridians and means of the deviatoric tracings at different levels of hydrostatic pressures.

Assuming the stress tensor as $\mathbf{T} = \sigma(K_1\mathbf{e}_1 \otimes \mathbf{e}_1 + K_2\mathbf{e}_2 \otimes \mathbf{e}_2 + K_3\mathbf{e}_3 \otimes \mathbf{e}_3)$, the maximum stresses, for monotonically increasing stress paths, are given on the two meridians in Eqs. (58)–(60) once the parameters are redefined.

(1) *Triaxial tensile stress state*

Tensile meridian: $K_1 = 1,\ K_2 = 1,\ K_3 > 1$;

Compressive meridian: $K_1 = 1,\ K_2 = 1,\ K_3 \in [0, 1]$;

the limit strength is given by Eq. (59) with obvious generalisation of the symbols.

(2) *Compressive–compressive–tensile stress state – tensile meridian*

$$K_1 = -1, \quad K_2 = -1, \quad K_3 > 0.$$

(3) *Tensile–tensile–compressive stress state – compressive meridian*

$$K_1 = 1, \quad K_2 = 1, \quad K_3 < 0.$$

The limit strength is given in both cases 2 and 3 by Eq. (59) once the parameters are redefined as

$$\beta = \sum_i K_i, \quad \psi^2 = \sum_i K_i^2, \quad \Gamma = \sqrt{\psi^2 - \frac{\beta^2}{3}}, \quad \zeta = \frac{1}{\sigma}\mathrm{tr}\,\mathbf{P}^* = \frac{1}{\sigma}\mathrm{tr}\,\mathbf{P},$$

$$\eta^{*2} = \frac{1}{\sigma^2}\sum_i \mathrm{P}_{ii}^{*2}, \quad \varphi^{*2} = -\frac{1}{\sigma}\sum_i K_i\mathrm{P}_{ii}^*, \quad \Pi = \sqrt{\psi^2 + \eta^{*2} + 2\varphi^{*2}},$$

while β, φ^2 and Γ are the same as defined for Eqs. (58)–(60).

(4) *Triaxial compressive stress state*

Tensile meridian: $K_1 = -1,\ K_2 = -1,\ K_3 \in [-1, 0]$;

Compressive meridian: $K_1 = -1,\ K_2 = -1,\ K_3 < -1$;

the limit strength is given by Eq. (60) with obvious generalisation of the symbols.

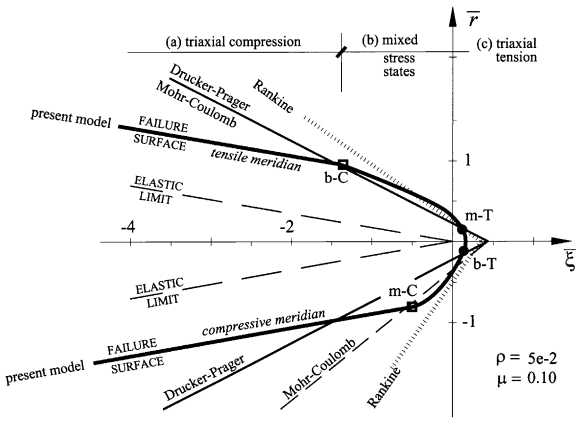

Fig. 15. Triaxial limit domain on the tensile ($\theta = 0°$) and compressive ($\theta = 60°$) meridians compared with Rankine, Mohr–Coulomb and Drucker–Prager surfaces.

Open cracks start to propagate when the limit condition (19) is attained at some orientation; otherwise cracks retain their original length and the local and global response remains linear elastic. From this point of view, the elastic limit under tensile stress states coincides with the failure limit. On compressed planes two limit conditions need to be attained to get failure: condition (19) and the friction limit (27). As already discussed in Section 3, there may be some stress state in which only one of these conditions is attained; on compressed planes, therefore, the limit for the elastic response does not coincide with the failure limit.

Figs. 15 and 16 represent the C^2-continuous failure envelope on the meridian plane and the envelope traces on the deviatoric plane for different values of the hydrostatic pressure. The model is able of representing the asymmetric shape of the two meridians for low values of the hydrostatic pressures, that is to say a higher resistance on the compressive meridian than on the tensile one; on the contrary, for triaxial compressive stress states, the Drucker–Prager type limit condition for sliding, Eq. (55), is attained, which corresponds to a circular cone in the space of principal stresses. The triple-symmetric cone section deforming in a circle for increasing values of the hydrostatic pressure is represented in Fig. 16.

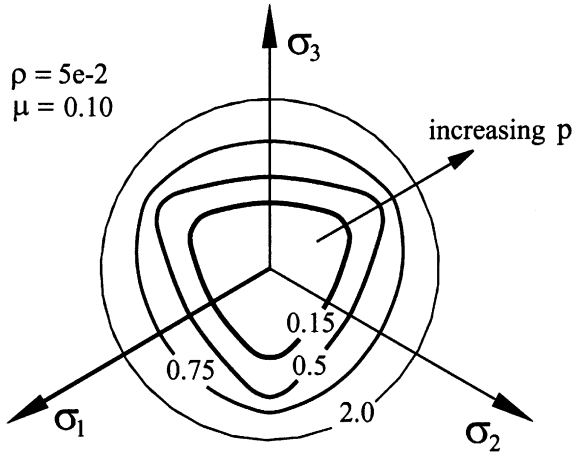

Fig. 16. Triaxial limit domain on the deviatoric plane for different values of the parameter $\bar{\xi}$.

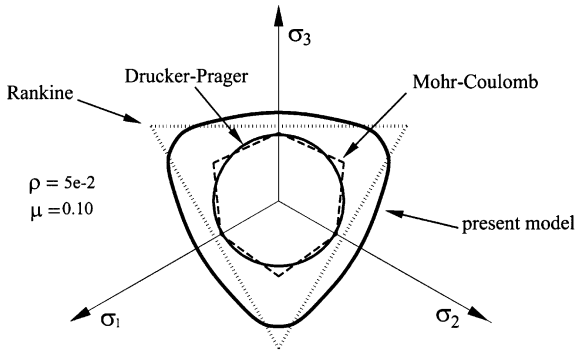

Fig. 17. Triaxial limit domain on the π plane for $\bar{\xi} = 0$ compared with Rankine, Mohr–Coulomb and Drucker–Prager surface traces.

In both Figs. 15 and 17 the traces of limit surface on tensile and compressive meridians are compared to the Rankine, Mohr–Coulomb and Drucker–Prager curves fitting the uniaxial strengths (on the tensile meridian the Mohr–Coulomb and Drucker–Prager surface traces coincide). Besides, in Fig. 15, also the elastic domain is represented where the relevant points indicated as m-T, m-C, b-T and b-C stand for the limit points for uniaxial and biaxial tension and compression respectively.

The stress states lying on the tensile and compressive meridian can be divided into three regions: (a) pure compressive stress states, (b) mixed stress states with both tensile and compression components, and (c) pure tensile states. The first two sections are nearly linear (exactly linear failure envelope for compressive stress states) with a sudden change in slope in the points corresponding to the uniaxial m-C and biaxial b-C compressive strengths (Fig. 15).

The analytical expressions given in the previous paragraph, Eqs. (26a), (26b), (56a) and (56b), show that only the limit stress for compressive stress states depends on the friction coefficient μ; the parametric representation of the failure surface on the meridian plane of Fig. 18 shows effects also on the tensile limit

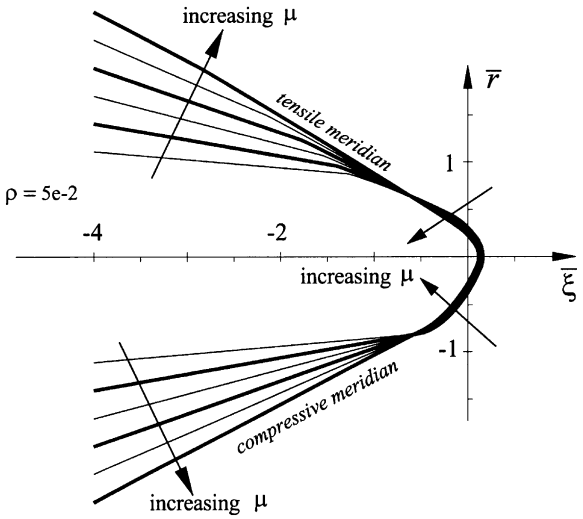

Fig. 18. Triaxial limit domain on the meridian section for fixed ρ and varying μ.

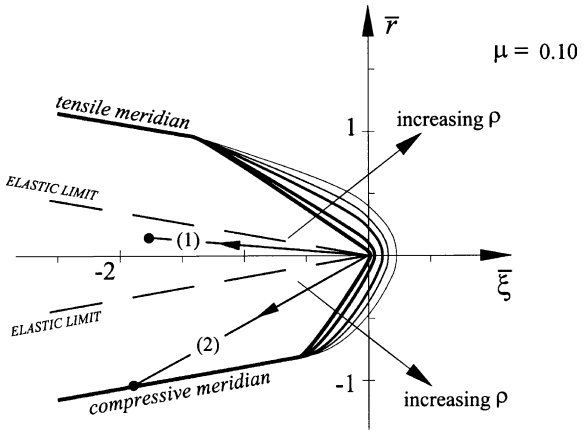

Fig. 19. Triaxial limit domain on the meridian plane for fixed μ and varying ρ: proportional loading path (1) inside the elastic domain and (2) up to the failure surface.

strength because of the normalising quantity (uniaxial compressive strength). An increase of the friction coefficient widens the failure cone in the full compressive stress states, as already conjectured from biaxial limit surfaces. Finally, the model parameter ρ has been defined as the ratio between the tangential and normal compliance, therefore it affects all the limit states in which some stress component is a tensile one, (Fig. 19.) In the same (Fig. 19) two different proportional loading paths are represented: path (1) is characterised by a low value of the tangential octahedral stress and remains inside the elastic domain; along path (2) the octahedral tangential stress is some 50% of the hydrostatic pressure and gets to failure when it intersects the failure domain.

Experimental data on triaxial strength of concrete-like materials point out, for low values of the hydrostatic pressure, a higher resistance on the compressive meridian than on the tensile one (Richard et al., 1928; Bellamy, 1961; Gardner, 1969; Mills and Zimmermann, 1970; Launay and Gachon, 1971). For compressive stress states this difference shrinks and the failure envelope tends to become a symmetric cone around the hydrostatic axis.

Comparison of the failure surface predicted by the model with experimental data, Figs. 20 and 21 for normal-strength concrete and Fig. 22 for high-strength concrete (Li and Ansari, 1999), points out a good approximation on the compressive meridian. Being the model limit condition for compressive stress states of a Drucker–Prager type, the failure surface is symmetrical for relevant hydrostatic compressions and, therefore, the model underestimates the material strength on the compressive meridian. It is worthwhile noting that the model fits quite well the failure envelope on the tensile meridian, with a precise prediction of the slope change from mixed stress states to pure compressive ones.

It has to be said that the values of the friction coefficient μ for triaxial limit domains are much higher than the values for biaxial domains: this is because the hydrostatic pressure component is quite low in the latter case, while triaxial tests are carried out for high values of the hydrostatic pressure, not less than half the uniaxial strength.

7. Conclusions

The local damage model presented in the paper is derived from a micromechanical description of the response of brittle materials and from some simplifying hypotheses aimed at reducing the number of in-

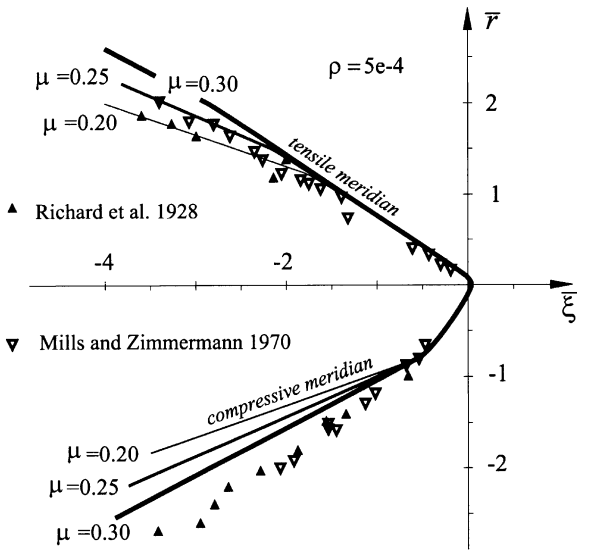

Fig. 20. Triaxial limit domain – data from Richard et al. (1928) and Mills and Zimmermann (1970).

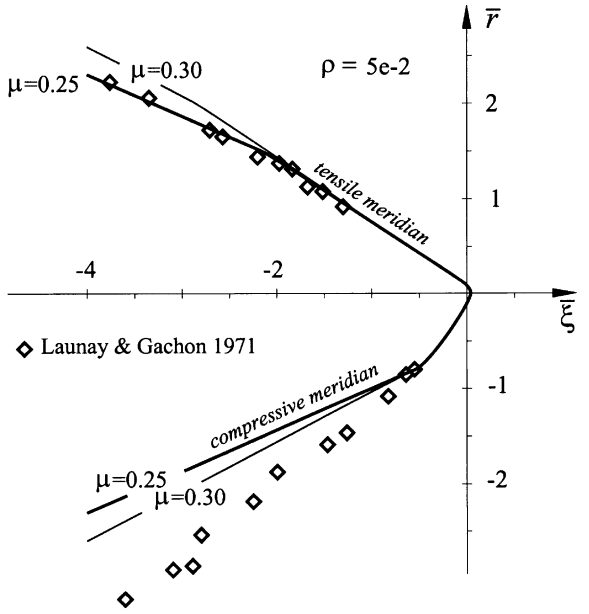

Fig. 21. Triaxial limit domain – data from Launay and Gachon (1971).

ternal variables. Damage is assumed to be isotropic as an overall measure of microcrack size and the effects of unilateral and frictional microcrack mechanisms are described by means of two second-order tensors. The latter represent, respectively, the average compressive stress on closed cracks and the frictional tractions that limit sliding, assumed without dilatancy. The evolution of the internal variables is ruled by a friction limit state coupled to a damage limit condition. The model is thus characterised by two parameters and a damage toughness function to be identified by means of experimental tests.

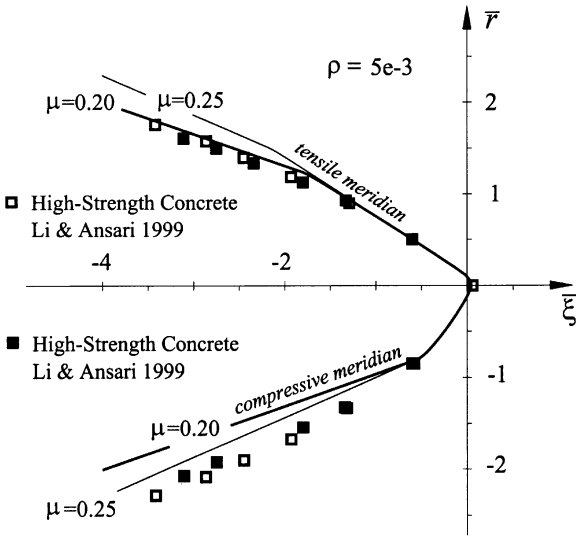

Fig. 22. Triaxial limit domain for high-strength concrete – data from Li and Ansari (1999).

In spite of the simplified approach, the model seems to represent the different response to tensile and compressive stress states of brittle materials both in terms of stress–strain response and of limit strength domains. The biaxial and triaxial strength domains fit rather well the experimental data and reproduce the relevant features of the failure surfaces. Less accuracy is found for triaxial compressive stress states, where on the compressive meridian the material strength is underestimated. This outcome, together with the inability of the model to describe damage and rupture under high hydrostatic compression, is a consequence of the basic inelastic mechanisms assumed for the model.

Finally, in spite of the simplifying assumption of isotropic damage, the present approach could be useful for deriving anisotropic damage models including different tensile–compressive response, as in Brencich and Gambarotta (1998).

Acknowledgements

This research was carried out with the financial support of the Department for University and Scientific and Technological Research (MURST) in the frame of the Joint Research Project "Structural integrity assessment of large dams".

References

Abu-Lebdeh, T.M., Voyiadjis, G.Z., 1993. Plasticity-damage model for concrete under cyclic multiaxial loading. ASCE J. Engng. Mech. 119, 1465–1484.

Adenaes, E., Gerstle, K.H., Ko, H.-Y., 1977. Response of mortar and concrete to biaxial compression. J. Engng. Mech. Div. 103, 515–526.

Basista, M., Gross, D., 1998. The sliding crack model of brittle deformation: an internal variable approach. Int. J. Solids Struct. 35, 487–509.

Bazant, Z.P., Prat, P.C., 1988. Microplane model for brittle-plastic materials: I – Theory; II – Verification. ASCE J. Engng. Mech. 110, 1672–1702.

Bellamy, C.J., 1961. Strength of concrete under combined stress. ACI J. 58, 367–381.
Brencich, A., Gambarotta, L., 1998. Anisotropic damage model for brittle materials with different tensile-compressive response. In: Murakami, H., Luco, J. (Eds.), Proc. 12th Engineering Mechanics Conference – ASCE Specialty Conference, La Jolla, May, 17–20 1998, pp. 889–892.
Chaboche, J.-L., 1992. Damage induced anisotropy: on the difficulties associated with the passive/active unilateral condition. Int. J. Damage Mech. 1, 148–171.
Chaboche, J.-L., 1993. Development of the continuum damage mechanics for elastic solids sustaining anisotropic and unilateral damage. Int. J. Damage Mech. 2, 311–329.
Chen, W.F., 1982. Plasticity in Reinforced Concrete. McGraw-Hill, New York.
Coffin, L.F., Schenectady, N.Y., 1950. The flow and fracture of a brittle material. J. Appl. Mech. 17, 233–248.
Cottle, R.W., Pang, J.-S., Stone, R.E., 1992. The Linear Complementarity Problem. Academic Press, New York.
Cornet, I., Grassi, R.C., 1955. Fracture of inoculated iron under biaxial stress. J. Appl. Mech. 22, 172–174.
Drucker, D.C., Prager, W., 1952. Soil mechanics and plastic analysis or limit design. Quart. Appl. Math. 10, 157–165.
Etse, G., Willam, K., 1995. Fracture energy formulation for inelastic behaviour of plain concrete. ASCE J. Engng. Mech. 120, 1983–2011.
Fanella, D., Krajcinovic, D., 1988. A micromechanical model for concrete in compression. Engng. Fract. Mech. 29, 49–66.
Gambarotta, L., Lagomarsino, S., 1993. A microcrack damage model for brittle materials. Int. J. Solids Struct. 30, 177–198.
Gardner, N.J., 1969. Triaxial behaviour of concrete. ACI J. 66, 136–146.
Halm, D., Dragon, A., 1998. Anisotropic model of damage and frictional sliding for brittle materials. Eur. J. Mech. A/Solids 17, 439–460.
Hansen, N.R., Schreyer, H.L., 1995. Damage activation. J. Appl. Mech. 62, 450–458.
Hsieh, S.S., Ting, E.C., Chen, W.F., 1982. A plastic-fracture model for concrete. Int. J. Solids Struct. 18, 181–197.
Kachanov, M., 1982. A microcrack model of rock inelasticity. Part I: Frictional sliding on microcracks. Part II: Propagation of microcracks. Mech. Mater. 1, 19–41.
Krajcinovic, D., Basista, M., Sumarac, D., 1991. Micromechanically inspired phenomenological damage model. J. Appl. Mech. 58, 305–310.
Krajcinovic, D., 1996. Damage Mechanics. Elsevier, Amsterdam.
Kupfer, H., Hilsdorf, H.K., Rusch, H., 1969. Behaviour of concrete under biaxial stress. ACI J. 66, 656–666.
Kupfer, H.B., Gerstle, K.H., 1973. Behaviour of concrete under biaxial stress. J. Engng. Mech. Div. 99, 853–866.
Launay, P., Gachon, H., 1971. Strain and ultimate strength of concrete under triaxial stress. ACI Special Publication 34, 13–43.
Lawn, B.R., Marshall, D.B., 1998. Non-linear stress–strain curves for solids containing closed cracks with friction. J. Mech. Phys. Solids 46, 85–113.
Lee, Y.-H., Willam, K.J., 1997. Anisotropic vertex plasticity formulation for concrete in plane stress. ASCE J. Engng. Mech. 123, 714–726.
Lemaitre, J., 1992. A Course on Damage Mechanics. Springer, Berlin.
Li, Q., Ansari, F., 1999. Mechanics of damage and constitutive relationships for high-strength concrete in triaxial compression. ASCE J. Engng. Mech. 125, 1–10.
Liu, T.C.Y., Nilson, A.H., Slate, F.O., 1972. Stress–strain response and fracture of concrete in uniaxial and biaxial compression. ACI J. 69, 291–295.
Lubarda, V.A., Krajcinovic, D., Mastilovic, S., 1994. Damage model for brittle elastic solids with unequal tensile and compressive strengths. Engng. Fract. Mech. 49, 681–697.
Lubliner, J, Oliver, J., Oller, S., Oñate, E., 1989. A plastic-damage model for concrete. Int. J. Solids Struct. 25, 299–326.
Maekawa, K., Okamura, H., 1983. The deformational behaviour and constitutive equation of concrete using the elasto-plastic and fracture model. J. of the Fac. of Eng. of Tokyo Univ., Series B37, 253.
Mills, L.L., Zimmerman, R.M., 1970. Compressive strength of plain concrete under multiaxial loading conditions. ACI J. 67, 802–807.
Nelissen, L.J.M., 1972. Biaxial testing of normal concrete. Heron 18, 1–90.
Nemat-Nasser, S., Obata, M., 1988. A microcrack model of dilatancy in brittle materials. J. Appl. Mech. 55, 24–35.
Ortiz, M., 1985. A constitutive theory for the inelastic behaviour of concrete. Mech. Mater. 4, 67–93.
Ouyang, C., Mobasher, B., Shah, S., 1990. An $\mathscr{R}$-curve approach for fracture of quasi-brittle materials. Engng. Fract. Mech. 37, 901–913.
Pietruszczak, S., Jiang, J., Mirza, F.A., 1988. An elasto-plastic constitutive model for concrete. Int. J. Solids Struct. 24, 705–722.
Prat, P.C., Bazant, Z.P., 1997. Tangential stiffness of elastic materials with systems of growing or closing cracks. J. Mech. Phys. Solids 45, 611–636.
Richard, F.E., Brandtzaeg, A., Brown, R.L., 1928. A study of the failure of concrete under combined compressive stresses. Bulletin of the University of Illinois, Urbana, Illinois, vol. 26, no. 12.
Tasuji, M.E., Slate, F.O., Nilson, A.H., 1978. Stress–strain response and fracture of concrete in biaxial loading. ACI J. 75, 306–312.

Thienel, K.C., Rostàsy, F.S., 1995. Strength of concrete subjected to high temperature and biaxial stress: experiments and modelling. Mater. Struct. 28, 575–581.

Weigler, H., Becker, G., 1961. Über das bruch- und verformungsverhalten von beton bei mehrachsiger beanspruchung. Der Bauingeneieur 36, 390–396.

Winnicki, A., Cichon, C., 1998. Plastic model for concrete in plane stress state. I: Theory; II: Numerical validation. ASCE J. Engng. Mech. 124, 591–613.

Yazdani, S., Schreyer, H.L., 1988. An anisotropic damage model with dilatation for concrete. Mech. Mater. 7, 231–244.

Yazdani, S., Schreyer, H.L., 1990. Combined plasticity and damage mechanics model for plain concrete. ASCE J. Engng. Mech. 116, 1435–1450.